

1 **Vertical resolution dependence of gravity wave momentum**
2 **flux simulated by an atmospheric general circulation model**

3 **S. Watanabe¹, K. Sato², Y. Kawatani¹, and M. Takahashi³**

4 [1]{Japan Agency for Marine-Earth Science and Technology, Yokohama, Japan}

5 [2]{Department of Earth and Planetary Science, Graduate School of Science, The University
6 of Tokyo, Tokyo, Japan}

7 [3]{Atmosphere and Ocean Research Institute, The University of Tokyo, Kashiwa, Japan}

8

9 Correspondence to: S. Watanabe (wnabe@jamstec.go.jp)

10

1 **Abstract**

2 The dependence of the gravity wave spectra of energy and momentum flux on the horizontal
3 resolution and time step of atmospheric general circulation models (AGCMs) has been
4 thoroughly investigated in the past. In contrast, much less attention has been given to the
5 dependence of these gravity wave parameters on models' vertical resolutions. The present
6 study demonstrates the dependence of gravity wave momentum flux (GWMF) in the
7 stratosphere and mesosphere on the model's vertical resolution, which is evaluated using an
8 AGCM with a horizontal resolution of about 0.56° . We performed a series of sensitivity test
9 simulations changing only the model's vertical resolution above a height of 8 km, and found a
10 global reduction of GWMF with increasing vertical resolution. Inertial gravity waves with
11 short vertical wavelengths simulated at higher vertical resolutions might play an important
12 role in determining GWMF in the summertime stratosphere. The sensitivity test simulation
13 also demonstrated the importance of model's vertical resolution on representing realistic
14 behaviors of gravity waves near their critical level.

15

1 **1 Introduction**

2 Due to recent advancements in high-performance computing, simulations of the global
3 atmosphere with sub-kilometer horizontal resolutions have been achieved, allowing
4 convective systems to be resolved (Miyamoto et al., 2013). Considering the global
5 momentum budget in such ultra high-resolution atmospheric models, explicitly resolved
6 gravity waves (GWs) undoubtedly play important roles (Alexander et al., 2010).

7 The dependence of the GW spectra of energy and momentum flux on the horizontal resolution
8 and time step of atmospheric general circulation models (AGCMs) has been studied in
9 considerable depth. Using comprehensive atmospheric general circulation models, Koshyk
10 and Hamilton (2001) and Hamilton et al. (2008) demonstrated the dependence of the
11 horizontal wavenumber spectra of GW energy on the horizontal resolution of the AGCM.
12 Shutts and Vosper (2011) evaluated the dependence of GW energy on the horizontal
13 resolution and time step of state-of-the-art numerical weather prediction models. These
14 pioneering works have served as useful guidance to other modeling disciplines.

15 In contrast, much less attention has been given to the dependence of the GW parameters on
16 the vertical resolution of the AGCM. At present, only a few AGCMs have achieved sub-
17 kilometer vertical resolution coverage throughout the middle atmosphere, which is believed to
18 be crucial for accurately reproducing GW-related processes such as generation, propagation,
19 dissipation, and mixing. Among such high-vertical-resolution AGCMs, the model developed
20 for the KANTO project had the highest vertical resolution of 300 m, which was actually
21 determined based on an expert judgment rather than a sensitivity test approach (Watanabe et
22 al., 2008). The main purpose of the present study is to clarify the dependence of GW
23 momentum flux on the vertical resolution of the model, with the aim of elucidating the
24 optimum vertical resolution.

25

26 **2 Model and experimental design**

27 The model used in the present study was JAGUAR (Japanese Atmospheric General
28 circulation model for Upper Atmosphere Research) (Watanabe and Miyahara, 2009). The
29 vertical domain of this model extends from the Earth's surface to a height of about 150 km,
30 although the present study focused on just the first 80 km. The horizontal resolution was set to
31 0.56° , which is the same as that used by Watanabe et al. (2008) and Watanabe and Miyahara

1 (2009). This horizontal resolution allows the model to resolve GWs with horizontal
2 wavelengths larger than ~ 190 km. Considering the fact that the GWs observed in the
3 mesosphere and lower thermosphere frequently include components with horizontal
4 wavelengths in the order of 10 km, the present model did not cover the full range of GW
5 spectra. Note, however, that a series of studies has suggested that the model qualitatively
6 reproduces the seasonal and interannual variations of large-scale thermal and wind structures,
7 behaviors of explicitly resolved GWs and vertically fine structures of the extratropical
8 tropopause layer (Watanabe et al., 2008, 2009; Tomikawa et al., 2008, 2012; Kawatani et al.,
9 2010a & b; Sato et al., 2009, 2012; Miyazaki et al., 2010a & b).

10

11 In the present study, we performed a series of sensitivity test simulations changing only the
12 model's vertical resolution above 8 km. Vertical resolutions of $dz = 200$ m, 300 m, 400 m,
13 500 m, and 1000 m were used (Figure A1). The vertical resolution below 8 km remained
14 unchanged. (Changing the vertical resolution in the lower troposphere is known to have
15 significant effects on the behaviors of physical parameterizations such as cumulus convection
16 and boundary layer processes, but these are not addressed in the present study.) The vertical
17 resolutions used in the KANTO project and the previous JAGUAR study were 300 and 500 m,
18 respectively. The main focus in this study was GW momentum flux at northern summer mid-
19 latitudes, where the short-term variability of planetary-scale and synoptic-scale waves is
20 relatively small. This condition is important because it is preferable for GW source
21 distribution (e.g., diabatic heating and jet-front systems) in the troposphere to be similar in
22 each run, to a qualitative degree at the very least.

23 Due to the limited computational resources available for this study, we only performed a
24 short-term deterministic forecast-type experiment starting from virtually the same initial
25 condition as in the original (control) simulation. The original initial condition at 00:00 UT on
26 June 21 was taken from a run using $dz = 500$ m, which had been spun-up for several years and
27 well reproduced large-scale thermal and wind structures in the middle atmosphere. That initial
28 condition was vertically interpolated into the $dz = 200$ m, 300 m, 400 m, and 1000 m runs,
29 each of which was performed for the week of June 21-27. The time step was set to 30 s in
30 every run.

31 Meteorological fields, e.g., winds, temperatures, and precipitations, were output every 30 min
32 as 30-min averages, and GW components were extracted using a high-pass filter based on the

1 spherical harmonics with a cut-off horizontal wavelength of about 950 km, i.e., wavelengths
2 shorter than 950 km were extracted (Watanabe et al., 2008). GW momentum flux is referred
3 to as GWMF hereafter for simplicity. This paper focuses on the net vertical flux of eastward
4 momentum associated with the GW components, because it is of primary importance in the
5 momentum budget in the middle atmosphere.

6 Both the chaotic behavior of the fluid system and the difference in the vertical resolution
7 resulted in different evolutions of the synoptic motions and GW distributions. However, as
8 will be shown later, the differences in the simulated GWMF in the middle atmosphere caused
9 by the vertical resolution were significant. Since the simulated GW field requires only a few
10 days for initial spin-up, i.e., to generate, propagate, and fill the stratosphere (Hamilton et al.,
11 2008; Shutts and Vosper, 2011) the present work mainly focused on the period of June 24-26,
12 during which the synoptic systems in all five runs held a morphological resemblance to each
13 other. Because the vertical interpolation used in the preparation of initial conditions disturbed
14 the original dynamical state, spurious GWs appeared during the initial spin-up, though we
15 found them to be negligible during the analysis period.

16

17 **3 Results**

18 **3.1 Strong dependence of GW momentum flux**

19 Figure 1a compares vertical profiles of the GWMF for northern summer mid-latitude, which
20 were simulated using the five different vertical resolutions. Positive values suggest the
21 dominance of the GWs propagating upward and eastward against background easterly winds
22 prevailing in the summertime stratosphere and mesosphere (e.g., Watanabe, 2008; Sato et al,
23 2009). It was quite surprising to find that the GWMF substantially decreases with increasing
24 vertical resolution throughout the stratosphere and mesosphere. In other words, a coarse
25 vertical resolution leads to a significant overestimation of the GWMF. This characteristic is
26 opposite to that for horizontal resolution; a coarse horizontal resolution causes an
27 underestimation of the GWMF, which results in a cold pole problem in the wintertime
28 stratosphere (Hamilton et al., 1999). In these particular simulations, the dependence of the
29 GWMF on the model's vertical resolution seems to start converging between $dz = 300$ m and
30 $dz = 200$ m. In the following sections, we discuss possible causes of this strong vertical
31 resolution dependence.

1 3.2 Critical level filtering

2 Figure 1b shows similar vertical profiles to Figure 1a but for the zonal mean zonal wind. The
3 wind profiles are almost identical to each other below 30 hPa, which implies that critical level
4 filtering of GWs propagating upward due to background large-scale flows in the troposphere
5 and lower stratosphere does not explain the differences in the GWMF. The difference in the
6 zonal mean zonal wind above the 30 hPa level rather reflects the difference in the GWMF,
7 that is, the larger GWMF in the coarser vertical resolution runs generally gives larger GW
8 forcing in the upper stratosphere and mesosphere, decelerating large-scale winds through
9 wave-mean flow interactions.

10 3.3 Effects of particular GW events

11 It is necessary to determine whether the present vertical resolution dependence of the GWMF
12 originates from particularly severe GW events. The upper panels of Figure 2 compare
13 longitude-height distributions of the net eastward GWMF for $dz = 1000$ m and 200 m. It is
14 revealed that the longitudinal distributions of large-scale zonal winds below the 30 hPa level
15 are qualitatively similar to each other. Meanwhile, the GWMF in the $dz = 1000$ m run is
16 generally larger than that in the $dz = 200$ m run. The GWMF is large not only near active
17 source regions, (100-160° E and 60-150° W), but also near relatively calm regions ($\pm 45^\circ$ from
18 0° E and near the date line). Although differences in the tropospheric circulation and locations
19 of convection in these two runs could account for the differences in the GWMF, we believe
20 that the systematic and global differences in the GWMF cannot solely be explained by them.

21 The lower panels of Figure 2 show the time evolution of the GWMF at the 30 hPa level, along
22 with contours of strong precipitation. Strong GW events with large positive GWMF (e.g.,
23 100-160° E) are repeatedly observed in the east of strong precipitation regions (e.g., 100-120°
24 E), suggesting that the GWMF is likely associated with convectively generated high
25 frequency GWs, which can penetrate westerly winds in the tropospheric subtropical jet (see
26 the contours of the background zonal winds in the upper panels). Overall, it can be concluded
27 that the vertical resolution dependence of the GWMF shown in Figure 1 is not caused by any
28 particular GW events, but is likely caused by systematic differences related to GW behaviors.

1 3.4 Effects of thin GWs

2 Sato et al. (1999) reported existence of a spectral peak of GWs near the inertial frequency in
3 the global lower stratosphere of a high-resolution (about 1° horizontal resolution) aqua-planet
4 AGCM experiment, which was later confirmed by observational evidence (Sato and Yoshiki,
5 2008). Such GWs have the lowest intrinsic frequency among vertically propagating GWs and
6 generally have short vertical wavelengths (e.g., less than 2-3 km). Therefore, a coarse vertical
7 resolution systematically reduces their number. Here, there is the apparent contradiction that
8 the GWMF *decreases* in runs with higher vertical resolutions, in which thin GWs can be
9 resolved.

10 Figure 3 shows close-up views of instantaneous longitude-height GW distributions (horizontal
11 wind divergence components). In the $dz = 200$ m run, thin GWs ($\lambda_z = 1-3$ km) which are
12 likely emitted by convective heating at around 140° E propagate upward and westward
13 against the tropospheric westerly jet. Qualitatively, these low-frequency GWs generated
14 within the sub-tropical jet reach their own critical levels near the zero-wind contours below a
15 50 hPa level, and do not directly affect the GWMF observed above the 30 hPa level.

16 As expected, the thin GWs ($\lambda_z = 1-3$ km) in the lower stratosphere are absent in the $dz = 1000$
17 m run. Instead, GWs with $\lambda_z > 4-5$ km are dominant everywhere, and the amplitude of the
18 GWs seen above the 30 hPa level is obviously larger than those in the $dz = 200$ m run.

19 Although the tropospheric circulation, distribution of moist diabatic heating, and phase
20 structures of GWs in the lower troposphere are not quite similar in the two runs, these
21 circumstances may imply the existence of suppression effects of the thin GWs in the $dz = 200$
22 m run, which effectively suppress the high-frequency GWs with longer vertical wavelengths.

23 One possible candidate of the suppression mechanisms is the parameterized turbulent
24 diffusion, which is not obviously seen in Figure 3 but sometime induced by wave saturation
25 of thin GWs. It is really hard to see but green lines in Figure 3 indicate regions of $Ri < 0.25$,
26 where parameterized turbulent mixing occurs in the model. The GWs with longer vertical
27 wavelength encountering the turbulent layer would be suppressed due to vertical
28 redistribution of wave momentum. Another suppression mechanism might be a discontinuous
29 vertical profiles of the buoyancy frequency, which causes the partial reflection of GWs (e.g.,
30 Sato et al. 2012).

31 -More statistical investigation are necessary to clarify the roles of thin GWs in the high-
32 vertical resolution models. One relevant study would be Lane and Knievel (2005), who

1 investigated the vertical resolution dependence of convectively generated GWs by using a
2 mesoscale model with much finer horizontal resolutions. Their study revealed that the
3 behavior of gravity waves as resolution is increased is not a straightforward monotonic
4 behavior.

書式変更: ドイツ語 (ドイツ)

5 3.5 Orographic GWs in the winter hemisphere

6 We have mainly focused on the non-orographic GWs appearing in the northern summer mid-
7 latitudes. Here we briefly investigate a case for orographic GWs in the southern winter mid-
8 latitudes. Figure 4 shows a similar longitude-height GW distributions to Figure 3, but over the
9 Andes. Westerly winds over the surface orography excite deep GWs, and their phase
10 structures resemble to each other below about 100 hPa. Above 100 hPa of the $dz = 200$ m run,
11 the vertical wavelength of orographic GWs substantially decreases with height and the GWs
12 disappear ~~below~~above about 30 hPa. This behavior suggests occurrences of Doppler shifting
13 and dissipation near the critical level associated with vertical variations of the background
14 winds. A weak wind layer is observed at 20-50 hPa downwind of the mountain, implying
15 effects of wave-mean flow interactions associated with the orographic GWs. On the other
16 hand, the minimum vertical wavelength of orographic GWs in the $dz = 1000$ m run ~~are not~~
17 ~~allowed to be shortened beyond the~~ is 2 km ~~limit~~, and they propagate higher than those seen in
18 the $dz = 200$ m run. The temporary and regional average of GWMF during this particular
19 orographic GW event in the $dz = 200$ m run was smaller than that in the $dz = 1000$ m run
20 throughout the troposphere and stratosphere (not shown). Although such dependence is
21 similar to the northern summer mid-latitudes, longer simulations and careful examinations are
22 needed since mountain waves have large intermittency, having just one case during the
23 present one week simulation.

24 3.6 Latitudinal variations

25 Figure 5 compares meridional distributions of the zonal mean zonal winds and GWMF, which
26 were simulated in the $dz = 1000$ m and $dz = 200$ m simulations. At almost all latitudes, the
27 magnitude of GWMF decreases with increasing vertical resolution, which in turn alters the
28 zonal mean wind structures through changes in GW forcing. Longer simulations are required
29 to obtain climatological views of the GWMF distributions and background wind structures,
30 and those dependence on the model's vertical resolution.

1
2
3
4
5
6
7
8
9
10
11
12
13
14
15
16
17
18
19
20
21
22
23
24
25
26
27
28
29
30

4 Concluding remarks

In order to investigate the vertical resolution dependence of the GWMF in a comprehensive AGCM which explicitly resolves a portion of the GW spectra ($\lambda_h > 190$ km), a series of sensitivity test simulations was performed changing only the model's vertical resolution ($dz = 200$ m, 300 m, 400 m, 500 m, and 1,000 m). The simulated GWMF in the stratosphere and mesosphere of northern summertime mid-latitude showed a strong dependence on the model's vertical resolution. The GWMF was systematically overestimated with decreasing vertical resolution; it was confirmed that this overestimation did not stem from any particular GW events. The existence of low-frequency thin ($\lambda_z = 1-3$ km) GWs in the lower stratosphere might cause the vertical resolution dependence of the GWMF. On the other hand, the case study for the deep orographic GWs in the southern wintertime mid-latitude showed the importance of vertical resolution on appropriate representation of wave phase tilting and dissipation near the critical level. The comparison for the meridional distribution of GWMF simulated with different vertical resolution confirmed that the GWMF in the middle atmosphere decreased with increasing vertical resolution at all latitudes. Further discussions and investigations are required to obtain plausible mechanisms that explain the causality of the present findings.

Author contribution

S. W. developed the model code. S. W. and K. S. designed the experiments, and S.W. carried them out. S.W. prepared the manuscript with contributions from all co-authors.

Acknowledgements

The authors would like to thank two anonymous referees for providing helpful comments on the original manuscript. This study was partly supported by a Grant-in-Aid for Scientific Research (A) 25247075 and the SOUSEI Program, MEXT, Japan. The numerical simulations in this study were performed using the Earth Simulator, and figures were drawn using GTOOL and the GFD-DENNOU Library.

1 **References**

2 Alexander, M. J., Geller, M., McLandress, C., Polavarapu, S., Preusse, P., Sassi, F., Sato, K.,
3 Eckermann, S., Ern, M., Hertzog, A., Kawatani, Y., Pulido, M., Shaw, T. A., Sigmond, M.,
4 Vincent, R., and Watanabe, S.: Recent developments in gravity-wave effects in climate
5 models and the global distribution of gravity-wave momentum flux from observations and
6 models, *Quarterly Journal of the Royal Meteorological Society*, n/a-n/a, 10.1002/qj.637, 2010.

7 Hamilton, K., Wilson, R. J., and Hemler, R. S.: Middle atmosphere simulated with high
8 vertical and horizontal resolution versions of a GCM: Improvements in the cold pole bias and
9 generation of a QBO-like oscillation in the tropics, *Journal of the Atmospheric Sciences*, 56,
10 3829-3846, 1999.

11 Hamilton, K., Takahashi, Y. O., and Ohfuchi, W.: Mesoscale spectrum of atmospheric
12 motions investigated in a very fine resolution global general circulation model, *Journal of*
13 *Geophysical Research*, 113, 10.1029/2008jd009785, 2008.

14 Koshyk, J. N., and Hamilton, K.: The horizontal kinetic energy spectrum and spectral budget
15 simulated by a high-resolution troposphere-stratosphere-mesosphere GCM, *Journal of the*
16 *Atmospheric Sciences*, 58, 329-348, 2001.

17 [Lane, T. P. and J. C. Knievel, Some effects of model resolution on simulated gravity waves
18 generated by deep, mesoscale convection, *J. Atmos. Sci.*, 2005, 62, p3408-3419.](#)

19 Miyamoto, Y., Kajikawa, Y., Yoshida, R., Yamaura, T., Yashiro, H., and Tomita, H.: Deep
20 moist atmospheric convection in a subkilometer global simulation, *Geophysical Research*
21 *Letters*, n/a-n/a, 10.1002/grl.50944, 2013.

22 Sato, K., and M. Yoshiki, Gravity wave generation around the polar vortex in the stratosphere
23 revealed by 3-hourly radiosonde observations at Syowa Station. *J. Atmos. Sci.*, 65, 3719-3735,
24 doi:10.1175/2008JAS2539.1, 2008.

25 Sato, K., Watanabe, S., Kawatani, Y., Tomikawa, Y., Miyazaki, K., and Takahashi, M.: On
26 the origins of mesospheric gravity waves, *Geophysical Research Letters*, 36, 2009.

27 Shutts, G. J., and Vosper, S. B.: Stratospheric gravity waves revealed in NWP model forecasts,
28 *Quarterly Journal of the Royal Meteorological Society*, 137, 303-317, 10.1002/qj.763, 2011.

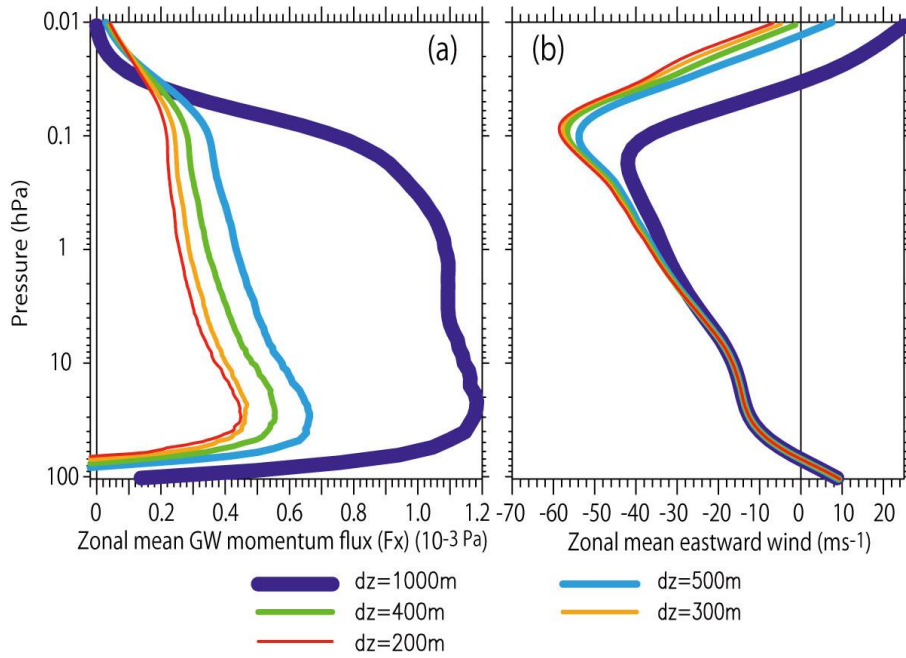
29 Watanabe, S.: Constraints on a Non-orographic Gravity Wave Drag Parameterization Using a
30 Gravity Wave Resolving General Circulation Model, *Sola*, 4, 61-64, 2008.

31 Watanabe, S., Kawatani, Y., Tomikawa, Y., Miyazaki, K., Takahashi, M., and Sato, K.:
32 General aspects of a T213L256 middle atmosphere general circulation model, *Journal of*
33 *Geophysical Research*, 113, 10.1029/2008jd010026, 2008.

34 Watanabe, S., and Miyahara, S.: Quantification of the gravity wave forcing of the migrating
35 diurnal tide in a gravity wave-resolving general circulation model, *J Geophys Res-Atmos*, 114,
36 2009.

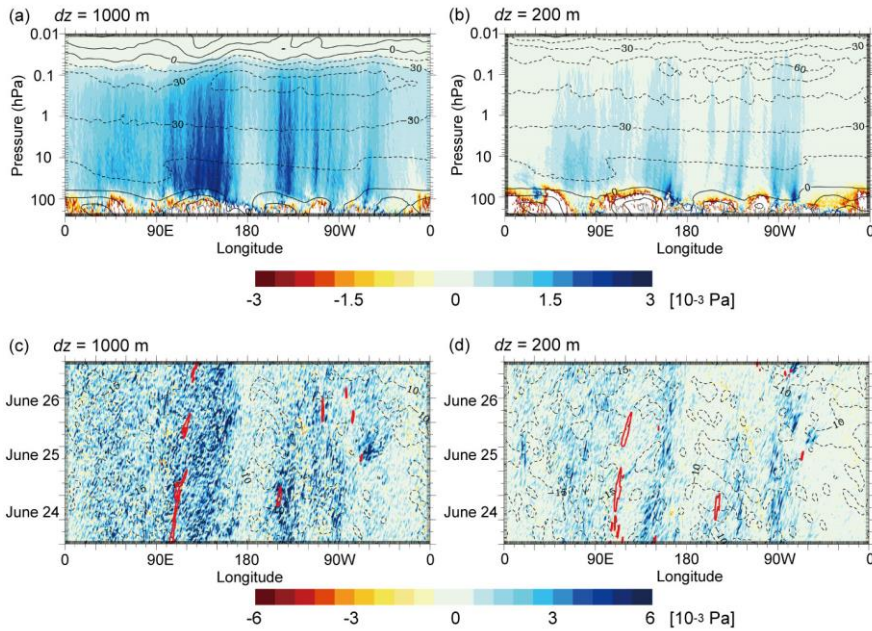
37

38



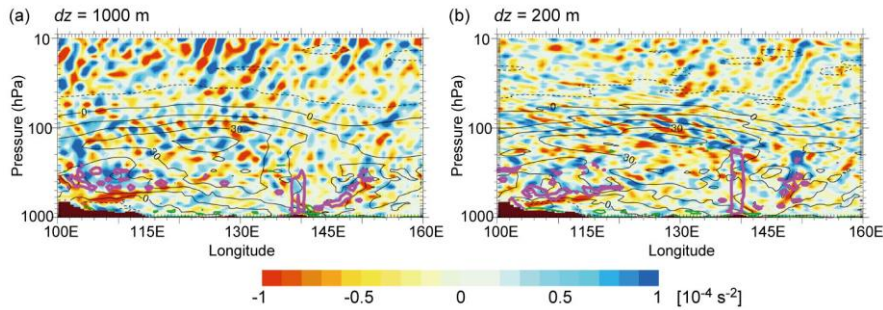
1
 2
 3 Figure 1. (a) Vertical profiles of the zonal mean net upward flux of the eastward momentum
 4 associated with the gravity wave component ($\lambda_h < 950$ km) for each vertical resolution. (b)
 5 Similar to (a) but for the zonal mean eastward winds. Averages over 35°N – 40°N from 00:00
 6 UT June 23 to 00:00 UT June 27 are shown.

7
 8



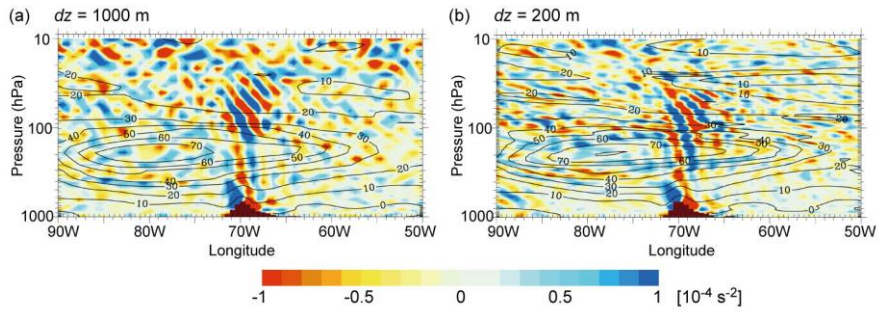
1
2 Figure 2. Upper panels: Longitude-height distribution of net upward flux of the eastward
3 momentum associated with the gravity wave component ($\lambda_h < 950$ km) in the $dz = 1000$ m run
4 (a) and $dz = 200$ m run (b). The contours show low-pass filtered (> 1000 km) eastward winds
5 with an interval of 15 ms^{-1} . Averages over $35^\circ \text{ N} - 40^\circ \text{ N}$ from 00:00 UT June 24 to 00:00 UT
6 June 27 are shown. Lower panels: Hovmöller diagrams of the eastward gravity wave
7 momentum flux (color) and the background large-scale eastward winds (black contours with
8 an interval of 5 ms^{-1}) at 30 hPa in the $dz = 1000$ m run (c) and $dz = 200$ m run (d). Red
9 contours show precipitation rate of 2 mm h^{-1} .

10

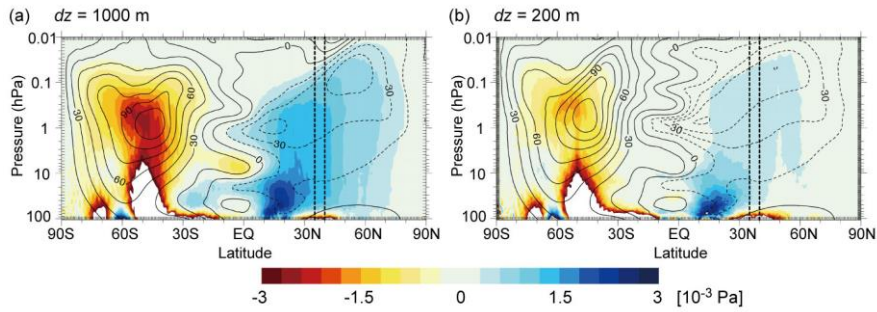


1
 2 Figure 3. Instantaneous longitude-height distribution of the unfiltered divergence component
 3 of the horizontal winds (color), the low-pass filtered (> 1000 km) eastward winds (black
 4 contours with an interval of 15 ms^{-1}) and the moist diabatic heating rate of 0.1 K h^{-1} (purple
 5 contours) at 37.5° N , 00:00 UT June 24. Green lines show regions of $Ri < 0.25$, where
 6 parameterized turbulent mixing occur in the model. Note that the longitudinal coverage is
 7 different from Figure 2.
 8

書式変更: フォント: 斜体

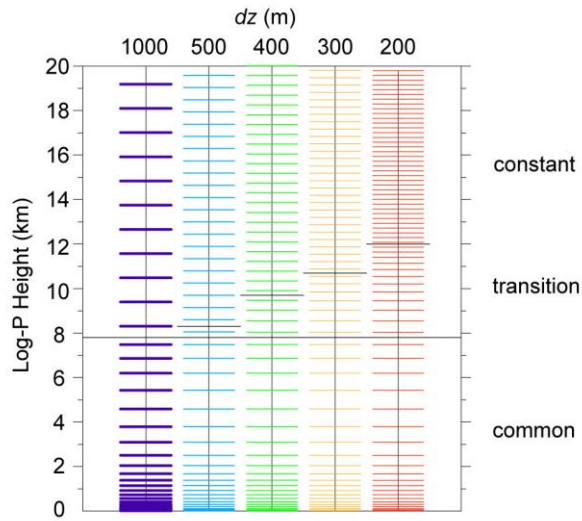


1
 2 Figure 4. Instantaneous longitude-height distribution of the unfiltered divergence component
 3 of the horizontal winds (color), the low-pass filtered (> 1000 km) eastward winds (black
 4 contours with an interval of 10 ms^{-1}) at 30° S , 06:00 UT June 27.
 5



1
 2 Figure 5. The zonal mean eastward winds (contours) and net upward flux of the eastward
 3 momentum associated with the gravity wave component ($\lambda_h < 950$ km) in the $dz = 1000$ m (a)
 4 and $dz = 200$ m (b) simulations. Averages from 00:00 UT June 23 to 00:00 UT June 27 are
 5 shown. The color shading with momentum flux larger than $\pm 3 \times 10^{-3}$ Pa are omitted. The
 6 latitude box of 35° N– 40° N is indicated, which we mainly focus in the present study.

7
 8



1
 2 Figure A1. Standard vertical layer distribution for each vertical resolution. Note that a hybrid
 3 sigma-pressure coordinate system was actually used in the model, and a scale height of 7 km
 4 was used to calculate the log-pressure standard levels shown in this figure.
 5